

Parametric instability analysis of a rotating shaft subjected to a periodic axial force by using discrete singular convolution method

Zhiwei Song · Zhigang Chen · Wei Li ·
Yingbin Chai

Received: 1 October 2015 / Accepted: 18 May 2016 / Published online: 23 May 2016
© Springer Science+Business Media Dordrecht 2016

Abstract Parametric instability problem of a rotating shaft subjected to a periodically varying axial force has been studied by using a numerical simulation method—discrete singular convolution. External viscous damping and internal material damping (Voigt–Kelvin model) have been considered. Parametric instability regions have been presented to illustrate the influence of spinning speed and damping. Numerical results reveal that for rotating shafts with no damping, parametric instability regions under different spinning speeds are ‘V’ shapes, and do not vary

obviously with spinning speed increasing. While, for rotating shafts with damping, parametric instability regions are enlarged significantly as spinning speed increases. It may be considered that spinning speed has a great effect on parametric instability of rotating shafts with damping, but little influence on that of rotating shafts with no damping. Moreover, the increase of damping results in reduction of parametric instability regions, which is helpful to improve dynamic stability of systems. And it is also found that effects of internal material damping and external viscous damping on parametric instability regions are similar. Compared to the results by using theoretical methods of Floquet and Bolotin, it is observed that the numerical results support Floquet’s method, disagree with Bolotin’s method for parametrically excited rotating shafts. In consideration of Bolotin’s method leading to enlargement of instability regions, it is strongly recommended that Bolotin’s should not be applied to parametric instability analysis of rotating systems.

Z. Song · W. Li (✉) · Y. Chai
School of Naval Architecture and Ocean Engineering,
Huazhong University of Science and Technology,
Wuhan 430074, China
e-mail: hustliw@hust.edu.cn

Z. Song
Urban Construction School, Wuchang Shouyi University,
Wuhan 430064, China

Z. Chen
China Ship Development and Design Center,
Wuhan 430064, China

W. Li
Hubei Key Laboratory of Naval Architecture and Ocean
Engineering Hydrodynamics (HUST), Wuhan 430074,
China

W. Li
Collaborative Innovation Center for Advanced Ship and
Deep-Sea Exploration (CISSE), Shanghai 200240, China

Keywords Parametric instability · Dynamic stability · Discrete singular convolution · Rotating shaft · Periodic axial force

1 Introduction

Parametric instability problem of rotating systems subjected to periodic axial forces has been an active

research issue and has been investigated by many researchers. Chen and Ku used finite element method to study dynamic stability of a rotating Timoshenko shaft [1], a rotating shaft embedded in an isotropic Winkler-type foundation [2] and a rotating Timoshenko shaft-disk system [3], respectively. Lee analyzed dynamic stability of spinning pre-twisted cantilever beams subjected to axial pulsating loads [4] and axial base excitations [5] by assumed mode method, respectively. Chen and Peng [6] studied dynamic stability of a rotating composite shaft under axial periodic forces by finite element method. Sheu and Chen [7] proposed a lumped mass model to study parametric instability of a cantilever shaft-disk system subjected to axial and follower loads. Lin and Chen [8] investigated dynamic stability of spinning pre-twisted sandwich beams with a constrained damping layer subjected to periodic axial loads. Other researchers [9–23] have also investigated vibration and dynamic stability of rotating systems.

Generally, when parametric instability problems are dealt with, the governing differential equations are reduced to a Mathieu–Hill equation, and the Mathieu–Hill equation determines boundaries of instability regions by using existing theoretical methods such as Bolotin [24], Floquet [18], and multiple scale method [10–12, 25] etc. In the most cases, results obtained by using Bolotin, Floquet and multiple scales method are coincident with each other except for some small errors. However, recently, Bolotin’s method is considered to lead to enlargement of instability regions for gyroscopic systems, and may contradict the results by using Floquet’s method [18], which is worthy of being focused on. To the authors’ knowledge, up till now, study on this problem has not been reported except the work of Pei [18]. In addition, it should be noted that when these theoretical methods are applied, parametric instability regions are determined by Mathieu–Hill equation. Whether another way to solve this problem exists or not is worth considering. Fortunately, another way [26] has been applied to analyze parametric instability problem, in which instability regions are determined by a direct simulation method, rather than the previously mentioned way. In the authors’ previous work [27–29], a direct simulation technique—discrete singular convolution (DSC) [30], has been successfully applied to analyze dynamic instability of beams. In the present work, this direct simulation technique is applied to parametric instability analysis

of a rotating shaft under a periodic axial force. And dynamic instability regions obtained by this direct way are compared to those by using theoretical methods of Bolotin and Floquet, which will further illustrate the contradiction between Bolotin and Floquet. Especially, to the authors’ knowledge, experimental reports on this problem have not been published. Therefore, the present numerical study appears especially important.

Discrete singular convolution (DSC) method proposed by Wei [31] has emerged as a new highly efficient technique for numerically solving differential equations. Although DSC method is considered as a local method, it has spectral level accuracy [32, 33]. Compared to other conventional numerical methods, this method has the global methods’ high level accuracy and the local methods’ flexibility for handling complex geometries and boundary conditions [34]. Like generalized differential quadrature (GDQ) method [35], DSC method can provide accurate solutions with relatively much fewer grid points. But DSC has some advantages over GDQ for solving higher-order vibration problems [34]. Compared to finite element method (FEM) [36], DSC method just need spatial discretization, and there are no real elements like the elements in FEM, which is quite different from FEM. Moreover, DSC method also can give extremely accurate and stable results for high-frequency vibration analysis of beams and plates [37, 38]. For more advantages of DSC for numerical solutions, readers may refer to published works of Wei et al. [30–34, 37–47]. DSC method has been successfully applied in vibration analysis of structures. Wei et al. [39–41] applied DSC method to vibration analysis of beams and plates with different boundary and internal support conditions [42–47], analysis and prediction of high-frequency vibrations [37, 38], and also explored matched interface boundary (MIB) method to treat free edges of plates [48]. Civalek used DSC method to solve vibration problems of thick rectangular plates [49], isotropic and orthotropic rectangular plates [50], laminated composite plates [51], rotating truncated conical shells [52], rotating laminated cylindrical shells [53] and laminated composite conical and cylindrical shells [54, 55]. Wang et al. [56] applied DSC method to vibration analysis of beams and rectangular plates with free edges, Timoshenko beams [57], thin isotropic and anisotropic rectangular plates [58], stepped beams [59] and plates

[60]. To extend the scope of DSC method, DSC-Ritz [61, 62] and DSC-element [63] method were explored for vibration analysis of thick plates, shallow shells, rectangular Mindlin plates. These studies indicate that DSC method works very well for vibration analysis of beams, plates and shells etc.

In vibration analysis of beams, plates and shells, DSC method is used to discretize the spatial derivatives and reduce the given partial differential equations into an eigenvalue problem [39–47]. However, for solutions of dynamic responses of beams or rotating shafts in time domain, the governing differential equations should be directly solved by DSC procedure [23, 27–29]. In the authors’ previous work [23], the governing differential equations of a rotating ship shaft under axial force have been solved by using DSC method. In that work, effects of number of blades in the propeller on parametric instability are focused on, and the exciting frequency of axial force is related to spinning speed, which is a very special case. For the most common cases, the exciting frequency of periodic axial force has no any relation with spinning speed such as those forces in the works of [1–4, 6–9, 12, 13]. Moreover, only external viscous damping is considered in the authors’ previous work [23] briefly. In fact, damping of rotating shafts includes external damping and internal material damping. Considering effects of internal material damping, the corresponding term relating to internal material damping is added to the governing differential equations of shafts, which complicate the equations. And DSC procedure for solving the problem considered here will be more complex than ever before.

This study extends the previous effort of the authors further to investigate parametric instability of rotating shafts under periodically varying axial forces by using DSC method which is completely different from theoretical methods of Floquet and Bolotin. A DSC procedure is given to solve the governing differential equations of a rotating Euler shaft under a periodic axial force. Influence of external viscous damping and internal material damping is also considered, and Voigt–Kelvin model [16] is used to describe the behavior of internal material damping. Parametric instability regions are presented to demonstrate the effects of spinning speed on rotating shafts without damping and with damping, respectively. Numerical results

obtained by using DSC procedure are compared to those by using theoretical methods.

2 Theoretical modal and algorithm

2.1 Equations of motion for rotating shafts

Figure 1 illustrates a uniform simply supported Euler shaft rotating about its longitudinal axis with a constant spinning speed Ω , subjected to a periodic axial force $P(t) = P_D \cos(\theta t)$, and (XYZ) is the fixed coordinate system while (xyz) is the coordinate system attached to the shaft with the x -axis aligned with the X -axis. Using Euler–Bernoulli beam theory, effect of rotatory inertia is neglected. The equations [9, 16] of motion can be written as

$$\begin{aligned}
 m \frac{\partial^2 u_y}{\partial t^2} - 2m\Omega \frac{\partial u_z}{\partial t} - m\Omega^2 u_y + C \frac{\partial u_y}{\partial t} + EI\alpha_i \frac{\partial^5 u_y}{\partial t \partial x^4} \\
 + EI \frac{\partial^4 u_y}{\partial x^4} + P(t) \frac{\partial^2 u_y}{\partial x^2} = 0 \\
 m \frac{\partial^2 u_z}{\partial t^2} + 2m\Omega \frac{\partial u_y}{\partial t} - m\Omega^2 u_z + C \frac{\partial u_z}{\partial t} + EI\alpha_i \frac{\partial^5 u_z}{\partial t \partial x^4} \\
 + EI \frac{\partial^4 u_z}{\partial x^4} + P(t) \frac{\partial^2 u_z}{\partial x^2} = 0
 \end{aligned} \tag{1}$$

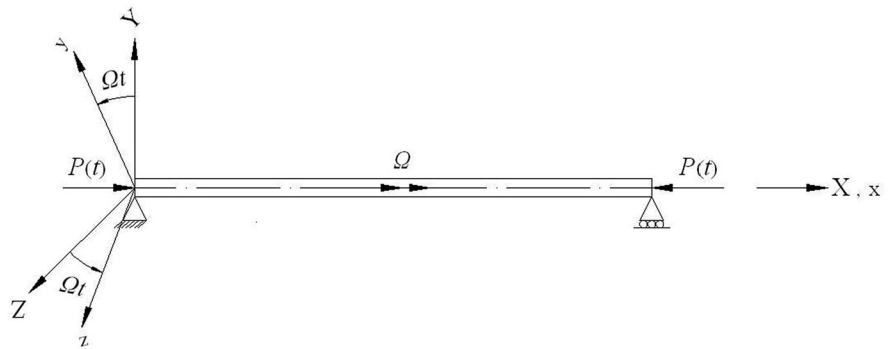
where u_y, u_z are the transverse displacements in the y - and z -direction, m, C, E, I, α_i and t are the mass per unit length, the viscous damping coefficient, Young’s modulus, the area moment of inertia, retardation time [16] and time, respectively. P_D and θ are the amplitude and circular frequency of the periodic axial force.

For simplicity, introducing following dimensionless quantities:

$$\begin{aligned}
 X = \frac{x}{l} \quad U_Y = \frac{u_y}{l} \quad U_Z = \frac{u_z}{l} \quad \alpha = \frac{P_D}{P_{cr}} \quad \bar{\Omega} = \frac{\Omega}{\omega} \\
 \Theta = \frac{\theta}{\omega} \quad \zeta_e = \frac{C}{2m\omega} \quad \zeta_i = \frac{\alpha_i}{2\omega} \quad \tau = \omega t \\
 U = \sqrt{U_Y^2 + U_Z^2}
 \end{aligned}$$

where l is the length, $P_{cr} = \pi^2 EI/l^2$ is the buckling force of a non-spinning simply supported shaft, $\omega = \pi^2 \sqrt{EI/ml^4}$ is the natural bending frequency of non-spinning shaft for the first mode, $\bar{\Omega}$ is dimensionless spinning speed, Θ is dimensionless exciting frequency, ζ_e is viscous damping ratio, ζ_i is reduced retardation time, U is the composition of U_Y and U_Z .

Fig. 1 The rotating shaft and coordinate systems



Then, Eq. (1) can be written as

$$\begin{aligned} \frac{\partial^2 U_Y}{\partial \tau^2} - 2\bar{\Omega} \frac{\partial U_Z}{\partial \tau} - \bar{\Omega}^2 U_Y + 2\zeta_e \frac{\partial U_Y}{\partial \tau} + \frac{2\zeta_i}{\pi^4} \frac{\partial^5 U_Y}{\partial \tau \partial X^4} \\ + \frac{1}{\pi^4} \frac{\partial^4 U_Y}{\partial X^4} + \frac{\alpha \cos(\Theta \tau)}{\pi^2} \frac{\partial^2 U_Y}{\partial \tau^2} = 0 \\ \frac{\partial^2 U_Z}{\partial \tau^2} + 2\bar{\Omega} \frac{\partial U_Y}{\partial \tau} - \bar{\Omega}^2 U_Z + 2\zeta_e \frac{\partial U_Z}{\partial \tau} + \frac{2\zeta_i}{\pi^4} \frac{\partial^5 U_Z}{\partial \tau \partial X^4} \\ + \frac{1}{\pi^4} \frac{\partial^4 U_Z}{\partial X^4} + \frac{\alpha \cos(\Theta \tau)}{\pi^2} \frac{\partial^2 U_Z}{\partial \tau^2} = 0 \end{aligned} \quad (2)$$

And Eq. (2) can be changed into

$$\begin{aligned} \frac{\partial^2 U_Y}{\partial \tau^2} = 2\bar{\Omega} \frac{\partial U_Z}{\partial \tau} + \bar{\Omega}^2 U_Y - 2\zeta_e \frac{\partial U_Y}{\partial \tau} \\ - \frac{2\zeta_i}{\pi^4} \frac{\partial^5 U_Y}{\partial \tau \partial X^4} - \frac{1}{\pi^4} \frac{\partial^4 U_Y}{\partial X^4} - \frac{\alpha \cos(\Theta \tau)}{\pi^2} \frac{\partial^2 U_Y}{\partial \tau^2} \\ \frac{\partial^2 U_Z}{\partial \tau^2} = -2\bar{\Omega} \frac{\partial U_Y}{\partial \tau} + \bar{\Omega}^2 U_Z - 2\zeta_e \frac{\partial U_Z}{\partial \tau} \\ - \frac{2\zeta_i}{\pi^4} \frac{\partial^5 U_Z}{\partial \tau \partial X^4} - \frac{1}{\pi^4} \frac{\partial^4 U_Z}{\partial X^4} - \frac{\alpha \cos(\Theta \tau)}{\pi^2} \frac{\partial^2 U_Z}{\partial \tau^2} \end{aligned} \quad (3)$$

The boundary conditions are

$$U(0, \tau) = U(1, \tau) = 0, \quad \frac{\partial^2 U(0, \tau)}{\partial X^2} = \frac{\partial^2 U(1, \tau)}{\partial X^2} = 0 \quad (4)$$

2.2 Discrete singular convolution and procedure

In the DSC algorithm originally introduced by Wei [30], the function $f(x)$ and its derivatives with respect to the x coordinate at a grid point x_i are approximated by a linear sum of discrete values $f(x_k)$ in a narrow bandwidth $[x - x_W, x + x_W]$. This expression can be written as follows [40, 53]

$$\left. \frac{d^n f(x)}{dx^n} \right|_{x=x_i} = f^{(n)}(x) \approx \sum_{k=-W}^W \delta_{\Delta, \sigma}^{(n)}(x_i - x_k) f(x_k) \quad (5)$$

$(n = 0, 1, 2, \dots)$

where superscript(n) denotes the n th-order derivative with respect to x and $2W + 1$ is the computational bandwidth which is centered around x and is usually smaller than the whole computational domain. δ is a singular kernel. The DSC algorithm can be realized by using many approximation kernels [45, 46]. Recently, an efficient kernel—regularized Shannon kernel (RSK) [37–40, 42, 43] was proposed to solve applied mechanic problems. The RSK is given as [39]

$$\delta_{\Delta, \sigma}(x - x_k) = \frac{\sin[(\pi/\Delta)(x - x_k)]}{(\pi/\Delta)(x - x_k)} \exp\left[-\frac{(x - x_k)^2}{2\sigma^2}\right], \quad \sigma > 0 \quad (6)$$

where Δ is the grid spacing. The parameter σ determines the width of the Gaussian envelope and often varies in association with the grid spacing, $\sigma = r\Delta$. Here r is a parameter chosen in computation. It is also known that the truncation error is very small due to the use of the Gaussian regularizer. When the regularized Shannon’s kernel is used, the detailed expressions for $\delta_{\Delta, \sigma}^{(n)}$ can be easily obtained. Readers may refer to some published references [40, 42, 44].

In solution procedure for governing differential equations of rotating shafts, the DSC discrete scheme Eq. (5) is utilized for the spatial discretization and the fourth-order Runge–Kutta (RK4) scheme is used for the time discretization [23, 27–29, 64]. The computational domain of coordinate X is $[0, 1]$, and the coordinate X is equally spaced, the grid sizes are denoted by $\Delta X = (1 - 0)/N$ (N is the total number of partition grid on the computational domain $[0, 1]$), the grid points are denoted by $X_j = (j - 1)\Delta X$ ($j = 1, 2, \dots, N + 1$). So $X_j - X_{j+k} = -k\Delta X$. The approximate values of U_Y and U_Z at the grid point X_j are

expressed as $U_{Y,i}$ and $U_{Z,i}$. Then, Eq. (2) can be expressed as

$$\begin{cases} \frac{\partial}{\partial \tau} \begin{bmatrix} U_{Y,j} \\ U_{Z,j} \end{bmatrix} = \begin{bmatrix} V_{Y,j} \\ V_{Z,j} \end{bmatrix} \\ \frac{\partial}{\partial \tau} \begin{bmatrix} V_{Y,j} \\ V_{Z,j} \end{bmatrix} = \begin{bmatrix} -2\zeta_e 2\bar{\Omega} \\ -2\bar{\Omega} - 2\zeta_e \end{bmatrix} \begin{bmatrix} V_{Y,j} \\ V_{Z,j} \end{bmatrix} \\ -\frac{2\zeta_i}{\pi^4} \frac{\partial}{\partial X^4} \begin{bmatrix} V_{Y,j} \\ V_{Z,j} \end{bmatrix} + \bar{\Omega}^2 \begin{bmatrix} U_{Y,j} \\ U_{Z,j} \end{bmatrix} \\ -\left(\frac{1}{\pi^4} \frac{\partial^4}{\partial X^4} + \frac{\alpha \cos(\Theta \tau)}{\pi^2} \frac{\partial^2}{\partial X^2} \right) \begin{bmatrix} U_{Y,j} \\ U_{Z,j} \end{bmatrix} \end{cases} \quad (7)$$

$(j = 1, 2, \dots, N + 1)$

Let

$$\begin{aligned} \{Y_{1,j}\} &= \{Y_{1,1}, Y_{1,2}, \dots, Y_{1,2N+2}\} \\ &= \{U_{Y,1}, U_{Y,2}, \dots, U_{Y,N+1}, V_{Y,1}, V_{Y,2}, \dots, V_{Y,N+1}\} \\ \{Y_{2,j}\} &= \{Y_{2,1}, Y_{2,2}, \dots, Y_{2,2N+2}\} \\ &= \{U_{Z,1}, U_{Z,2}, \dots, U_{Z,N+1}, V_{Z,1}, V_{Z,2}, \dots, V_{Z,N+1}\} \end{aligned}$$

$(j = 1, 2, \dots, 2N + 2)$

When $j = 1, 2, \dots, N + 1$

$$F_{i,j} = Y_{i,j+N+1} \quad (i = 1, 2) \quad (8)$$

and when $j = N + 2, N + 3, \dots, 2N + 2$

$$\begin{cases} \begin{bmatrix} F_{1,j} \\ F_{2,j} \end{bmatrix} = \begin{bmatrix} -2\zeta_e 2\bar{\Omega} \\ -2\bar{\Omega} - 2\zeta_e \end{bmatrix} \begin{bmatrix} Y_{1,j} \\ Y_{2,j} \end{bmatrix} \\ -\frac{2\zeta_i}{\pi^4} \frac{\partial}{\partial X^4} \begin{bmatrix} Y_{1,j} \\ Y_{2,j} \end{bmatrix} + \bar{\Omega}^2 \begin{bmatrix} Y_{1,j-N-1} \\ Y_{2,j-N-1} \end{bmatrix} \\ -\left(\frac{1}{\pi^4} \frac{\partial^4}{\partial X^4} + \frac{\alpha \cos(\Theta \tau)}{\pi^2} \frac{\partial^2}{\partial X^2} \right) \begin{bmatrix} Y_{1,j-N-1} \\ Y_{2,j-N-1} \end{bmatrix} \end{cases} \quad (9)$$

Then, we have a unified semi-discretized equation.

$$\frac{\partial Y_{i,j}}{\partial \tau} = F_{i,j} \quad (i = 1, 2, j = 1, 2, \dots, 2N + 2) \quad (10)$$

The temporal discretization expressions of Eq. (10) by using fourth-order Runge–Kutta method are given as

$$\begin{aligned} Y_{i,j}^{n+1} &= Y_{i,j}^n + \Delta \tau Y_{i,j+N+1}^n + \frac{\Delta \tau^2}{6} (L_{i,j+N+1,1} \\ &\quad + L_{i,j+N+1,2} + L_{i,j+N+1,3}) \end{aligned} \quad (11)$$

$(i = 1, 2, j = 1, 2, \dots, N + 1)$

$$\begin{aligned} Y_{i,j}^{n+1} &= Y_{i,j}^n + \frac{\Delta \tau}{6} (L_{i,j,1} + 2L_{i,j,2} + 2L_{i,j,3} + L_{i,j,4}) \\ &\quad (i = 1, 2, j = N + 2, N + 3, \dots, 2N + 2) \end{aligned} \quad (12)$$

where $L_{i,j,1} = F_{i,j,1}^n, L_{i,j,2} = F_{i,j,2}^n, L_{i,j,3} = F_{i,j,3}^n, L_{i,j,4} = F_{i,j,4}^n (i = 1, 2, j = N + 2, N + 3, \dots, 2N + 2)$, and here superscript n denotes time level, $\Delta \tau$ is the time step, so $\tau = n\Delta \tau$. Using DSC discrete scheme Eq. (5), the discretization expressions for $F_{i,j,1}^n, F_{i,j,2}^n, F_{i,j,3}^n, F_{i,j,4}^n$ are

$$\begin{aligned} \begin{cases} \begin{bmatrix} L_{1,j,1} \\ L_{2,j,1} \end{bmatrix} &= \begin{bmatrix} F_{1,j,1}^n \\ F_{2,j,1}^n \end{bmatrix} = \begin{bmatrix} -2\zeta_e 2\bar{\Omega} \\ -2\bar{\Omega} - 2\zeta_e \end{bmatrix} \begin{bmatrix} Y_{1,j}^n \\ Y_{2,j}^n \end{bmatrix} \\ -\frac{2\zeta_i}{\pi^4} \sum_{k=-W}^{+W} \delta_{\Delta,\sigma}^{(4)}(-k\Delta X) \begin{bmatrix} Y_{1,j+k}^n \\ Y_{2,j+k}^n \end{bmatrix} + \bar{\Omega}^2 \begin{bmatrix} Y_{1,j-N-1}^n \\ Y_{2,j-N-1}^n \end{bmatrix} \\ -\left(\frac{1}{\pi^4} \sum_{k=-W}^{+W} \delta_{\Delta,\sigma}^{(4)}(-k\Delta X) + \frac{\alpha \cos(\Theta \tau)}{\pi^2} \sum_{k=-W}^{+W} \delta_{\Delta,\sigma}^{(2)}(-k\Delta X) \right) \\ \times \begin{bmatrix} Y_{1,j+k-N-1}^n \\ Y_{2,j+k-N-1}^n \end{bmatrix} \end{cases} \begin{cases} \begin{bmatrix} L_{1,j,2} \\ L_{2,j,2} \end{bmatrix} &= \begin{bmatrix} F_{1,j,2}^n \\ F_{2,j,2}^n \end{bmatrix} \\ = \begin{bmatrix} -2\zeta_e 2\bar{\Omega} \\ -2\bar{\Omega} - 2\zeta_e \end{bmatrix} \begin{bmatrix} Y_{1,j}^n + (\Delta \tau/2)L_{1,j,1} \\ Y_{2,j}^n + (\Delta \tau/2)L_{2,j,1} \end{bmatrix} \\ -\frac{2\zeta_i}{\pi^4} \sum_{k=-W}^{+W} \delta_{\Delta,\sigma}^{(4)}(-k\Delta X) \begin{bmatrix} Y_{1,j+k}^n + (\Delta \tau/2)L_{1,j+k,1} \\ Y_{2,j+k}^n + (\Delta \tau/2)L_{2,j+k,1} \end{bmatrix} \\ + \bar{\Omega}^2 \begin{bmatrix} Y_{1,j-N-1}^n + (\Delta \tau/2)Y_{1,j}^n \\ Y_{2,j-N-1}^n + (\Delta \tau/2)Y_{2,j}^n \end{bmatrix} \\ -\left(\frac{1}{\pi^4} \sum_{k=-W}^{+W} \delta_{\Delta,\sigma}^{(4)}(-k\Delta X) + \frac{\alpha \cos(\Theta \tau)}{\pi^2} \sum_{k=-W}^{+W} \delta_{\Delta,\sigma}^{(2)}(-k\Delta X) \right) \\ \times \begin{bmatrix} Y_{1,j+k-N-1}^n + (\Delta \tau/2)Y_{1,j+k}^n \\ Y_{2,j+k-N-1}^n + (\Delta \tau/2)Y_{2,j+k}^n \end{bmatrix} \end{cases} \\ \begin{cases} \begin{bmatrix} L_{1,j,3} \\ L_{2,j,3} \end{bmatrix} &= \begin{bmatrix} F_{1,j,3}^n \\ F_{2,j,3}^n \end{bmatrix} = \begin{bmatrix} -2\zeta_e 2\bar{\Omega} \\ -2\bar{\Omega} - 2\zeta_e \end{bmatrix} \\ \times \begin{bmatrix} Y_{1,j}^n + (\Delta \tau/2)L_{1,j,2} \\ Y_{2,j}^n + (\Delta \tau/2)L_{2,j,2} \end{bmatrix} - \frac{2\zeta_i}{\pi^4} \sum_{k=-W}^{+W} \delta_{\Delta,\sigma}^{(4)}(-k\Delta X) \\ \times \begin{bmatrix} Y_{1,j+k}^n + (\Delta \tau/2)L_{1,j+k,2} \\ Y_{2,j+k}^n + (\Delta \tau/2)L_{2,j+k,2} \end{bmatrix} \\ + \bar{\Omega}^2 \begin{bmatrix} Y_{1,j-N-1}^n + (\Delta \tau/2)Y_{1,j}^n + (\Delta \tau^2/4)L_{1,j,1} \\ Y_{2,j-N-1}^n + (\Delta \tau/2)Y_{2,j}^n + (\Delta \tau^2/4)L_{2,j,1} \end{bmatrix} \\ -\left(\frac{1}{\pi^4} \sum_{k=-W}^{+W} \delta_{\Delta,\sigma}^{(4)}(-k\Delta X) + \frac{\alpha \cos(\Theta \tau)}{\pi^2} \sum_{k=-W}^{+W} \delta_{\Delta,\sigma}^{(2)}(-k\Delta X) \right) \\ \times \begin{bmatrix} Y_{1,j+k-N-1}^n + (\Delta \tau/2)Y_{1,j+k}^n + (\Delta \tau^2/4)L_{1,j+k,1} \\ Y_{2,j+k-N-1}^n + (\Delta \tau/2)Y_{2,j+k}^n + (\Delta \tau^2/4)L_{2,j+k,1} \end{bmatrix} \end{cases} \end{cases}$$

$$\begin{aligned} & \left\{ \begin{matrix} L_{1,j,4} \\ L_{2,j,4} \end{matrix} \right\} = \begin{bmatrix} F_{1,j,4}^n \\ F_{2,j,4}^n \end{bmatrix} = \begin{bmatrix} -2\zeta_e 2\bar{\Omega} \\ -2\bar{\Omega} - 2\zeta_e \end{bmatrix} \begin{bmatrix} Y_{1,j}^n + \Delta\tau L_{1,j,3} \\ Y_{2,j}^n + \Delta\tau L_{2,j,3} \end{bmatrix} \\ & - \frac{2\zeta_i}{\pi^4} \sum_{k=-W}^{+W} \delta_{\Delta,\sigma}^{(4)}(-k\Delta X) \begin{bmatrix} Y_{1,j+k}^n + \Delta\tau L_{1,j+k,3} \\ Y_{2,j+k}^n + \Delta\tau L_{2,j+k,3} \end{bmatrix} \\ & + \bar{\Omega}^2 \begin{bmatrix} Y_{1,j-N-1}^n + \Delta\tau Y_{1,j}^n + (\Delta\tau^2/2)L_{1,j,2} \\ Y_{2,j-N-1}^n + \Delta\tau Y_{2,j}^n + (\Delta\tau^2/2)L_{2,j,2} \end{bmatrix} \\ & - \left(\frac{1}{\pi^4} \sum_{k=-W}^{+W} \delta_{\Delta,\sigma}^{(4)}(-k\Delta X) + \frac{\alpha \cos(\Theta \tau)}{\pi^2} \sum_{k=-W}^{+W} \delta_{\Delta,\sigma}^{(2)}(-k\Delta X) \right) \\ & \times \begin{bmatrix} Y_{1,j+k-N-1}^n + \Delta\tau Y_{1,j+k}^n + (\Delta\tau^2/2)L_{1,j+k,2} \\ Y_{2,j+k-N-1}^n + \Delta\tau Y_{2,j+k}^n + (\Delta\tau^2/2)L_{2,j+k,2} \end{bmatrix} \\ & (j=N+2, N+3, \dots, 2N+2). \end{aligned} \tag{13}$$

where $[-W, +W]$ is the computational bandwidth. Kernels $\delta_{\Delta,\sigma}^{(2)}$ and $\delta_{\Delta,\sigma}^{(4)}$ can be easily obtained [40, 42, 44]. All of these coefficients are only dependent on grid size. When the grid point distribution is given, the coefficients can be computed once and stored for use during the computation.

The overall calculation procedure can be summarized as follows [23, 27–29]:

- (a) with the initial values for Y_{ij}^0 or the values of Y_{ij}^n ($i = 1, 2, j = 1, 2, \dots, 2N + 2$) at previous time level n . And the values beyond the computational domain can be obtained by anti-symmetric extension according to simply supported boundary [45];
- (b) values of $F_{i,j,1}^n, F_{i,j,2}^n, F_{i,j,3}^n, F_{i,j,4}^n$ ($i = 1, 2, j = N + 2, N + 3, \dots, 2N + 2$) at the time level n can be obtained from Eq. (13);
- (c) substituting the values in Eq. (13) into Eqs. (11) and (12), values of Y_{ij}^{n+1} ($i = 1, 2, j = 1, 2, \dots, 2N + 2$) at new time level $n + 1$ can be calculated;
- (d) the computational time is advanced (i.e. $\tau = \tau + \Delta\tau, n = n + 1$), and the whole procedure above is repeated, until calculation precision is reached.

3 Numerical results and discussions

In this section, parametric instability regions for the first mode of a rotating shaft with different spinning

speeds under a periodic axial force are presented. Effects of spinning speed on instability regions of rotating shaft without damping and with external viscous and internal material damping are also discussed, respectively.

3.1 Parametric instability regions for shafts with no damping

In order to discuss effects of spinning speed on parametric instability regions for shafts with no damping, values of different spinning speeds $\bar{\Omega}$ are chosen as 0.3, 0.5, 0.7. The initial conditions and parameters in DSC algorithm are set: $U_Y(i\Delta X, 0) = 0.001 \sin(i\Delta X\pi)$, $U_Z(i\Delta X, 0) = 0$, $\partial U_Y(i\Delta X, 0)/\partial\tau = \partial U_Z(i\Delta X, 0)/\partial\tau = 0$ ($i = 0, 1, 2, \dots, N$), $N = 16$, $W = 15$, $r = 2.5$, $\Delta\tau = 3.0 \times 10^{-6}$. For the choice of N , W and r , readers may refer to the works of [40, 42, 65].

Figure 2 shows dynamic responses of dimensionless displacements at midpoint for a rotating shaft with no damping and spinning speed $\bar{\Omega} = 0.3$. It is observed that the dynamic responses for $\theta/2\omega = 1.0$ $\alpha = 0.05$, $\theta/2\omega = 0.9$ $\alpha = 0.40$ and $\theta/2\omega = 1.1$ $\alpha = 0.42$ in Fig. 2a, c, e, are dynamically unstable; while the dynamic responses for $\theta/2\omega = 0.9$ $\alpha = 0.38$ and $\theta/2\omega = 1.1$ $\alpha = 0.40$ in Fig. 2b, d, are dynamically stable. The whole procedure above is repeated, then the principal parametric instability region for the first mode shown as Fig. 3 is plotted. It is found that the parametric instability region determined by DSC algorithm is coincident with that determined by Floquet’s method [18] very well. The parametric instability region is ‘V’ shape, and when the exciting frequency is twice of the natural bending frequency of non-spinning shaft ($\theta/2\omega = 1.0$), the parametric instability is the most serious.

Similarly, parametric instability regions with different spinning speeds $\bar{\Omega} = 0.5$ and 0.7 for a rotating shaft with no damping are plotted in Figs. 4 and 5. It is observed from these figures that parametric instability regions determined by DSC algorithm are in good agreement with those determined by Floquet’s method, respectively, which verifies applicability of DSC algorithm to parametric instability analysis of rotating shafts. And all the parametric instability regions are ‘V’ shapes. It is also seen that there are some errors in these figures, especially when the value

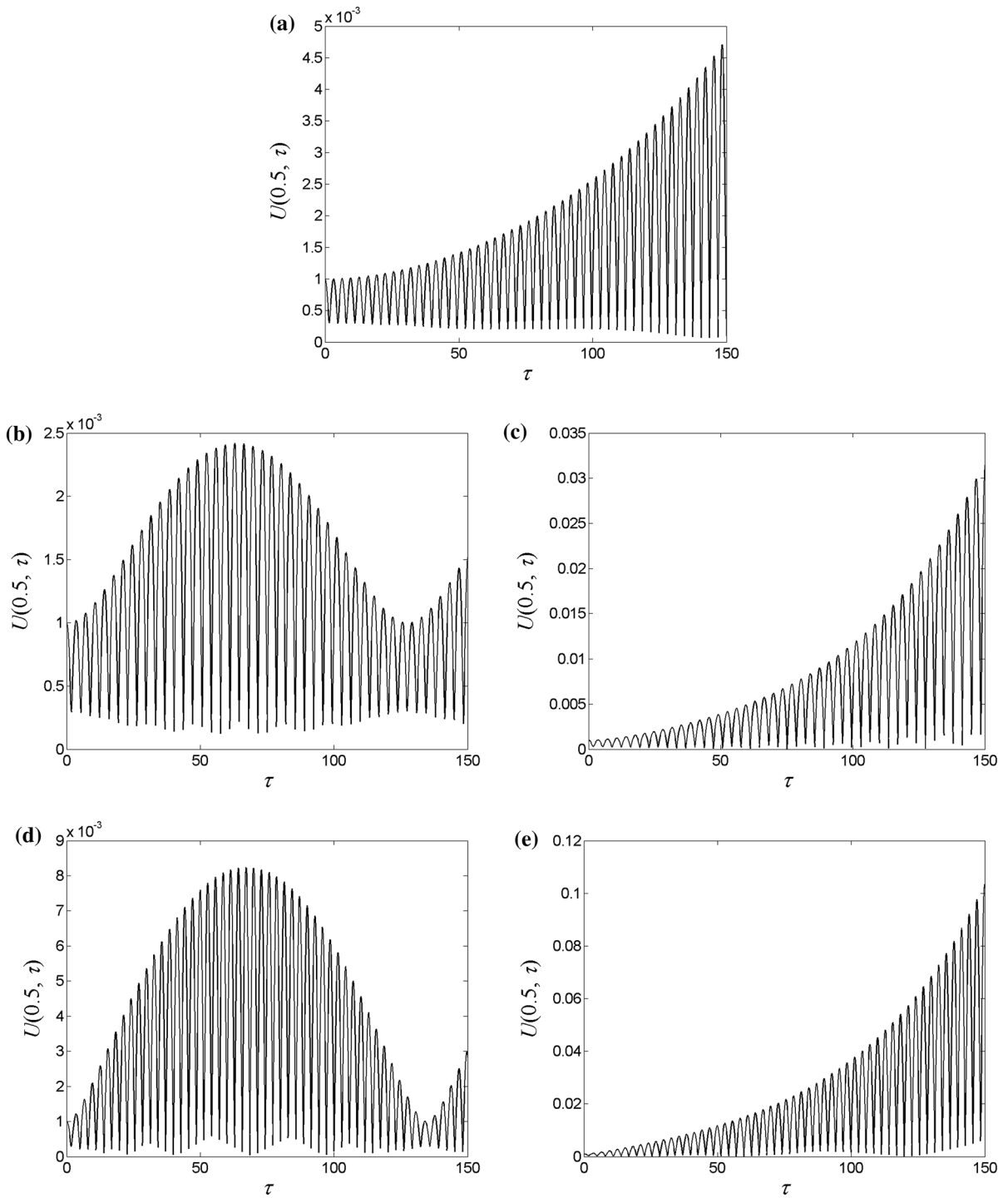


Fig. 2 Dynamic responses of dimensionless displacements for a rotating shaft with no damping and spinning speed $\bar{\Omega} = 0.3$. **a** $\theta/2\omega = 1.0, \alpha = 0.05$, **b** $\theta/2\omega = 0.9, \alpha = 0.38$, **c** $\theta/2\omega = 0.9, \alpha = 0.40$, **d** $\theta/2\omega = 1.1, \alpha = 0.40$, **e** $\theta/2\omega = 1.1, \alpha = 0.42$

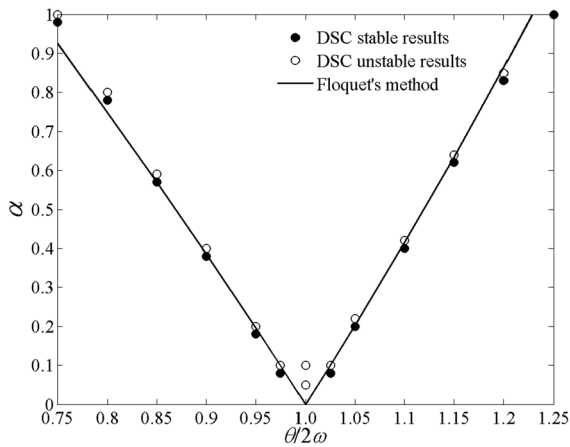


Fig. 3 Parametric instability region for a rotating shaft with no damping and spinning speed $\bar{\Omega} = 0.3$

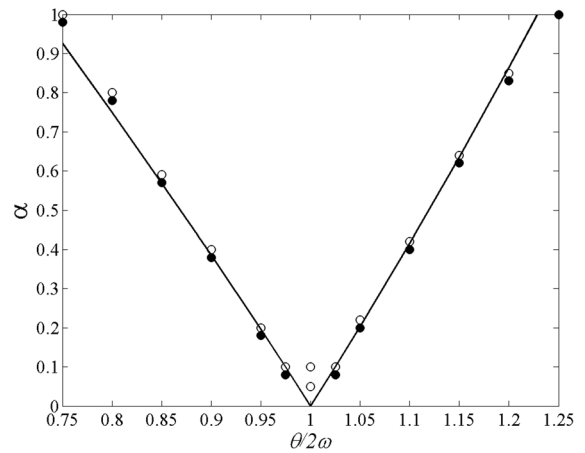


Fig. 5 As Fig. 3, but $\bar{\Omega} = 0.7$, Key as for Fig. 3

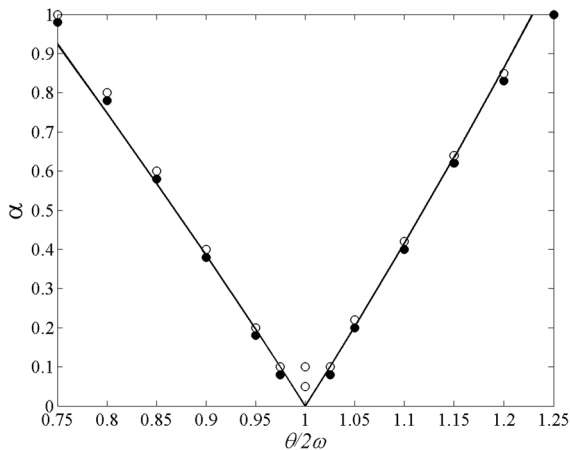


Fig. 4 As Fig. 3, but $\bar{\Omega} = 0.5$, Key as for Fig. 3

of α is very large. The reasons for obvious errors are that the first approximation [18] of Floquet's method and assumed mode method are applied to determine the boundaries of instability regions. Due to neglecting the second and higher-order terms, when the value of the axial force (α) is very large, the application of the first approximation will result in obvious error. Moreover, the assumed mode is not the real mode of the shaft subjected to a periodic axial force. The difference of assumed mode and real mode gets very obvious with large value of α , which also lead to obvious error.

A comparison of parametric instability regions with different spinning speeds for a rotating shaft with no damping is shown in Fig. 6, and instability regions

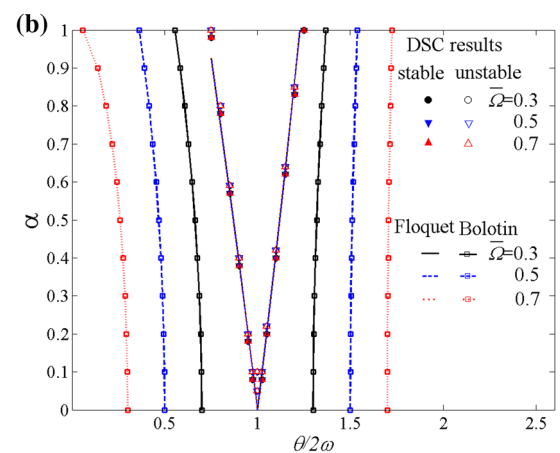
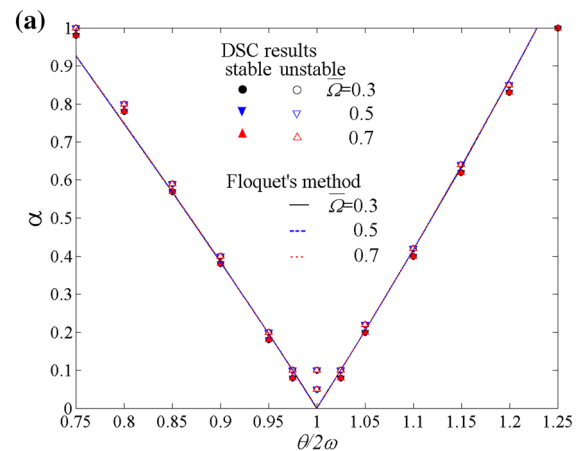


Fig. 6 Effects of spinning speed on parametric instability regions for a rotating shaft with no damping. **a** Parametric instability regions by DSC and Floquet's methods, **b** parametric instability regions by DSC, Floquet's and Bolotin's methods

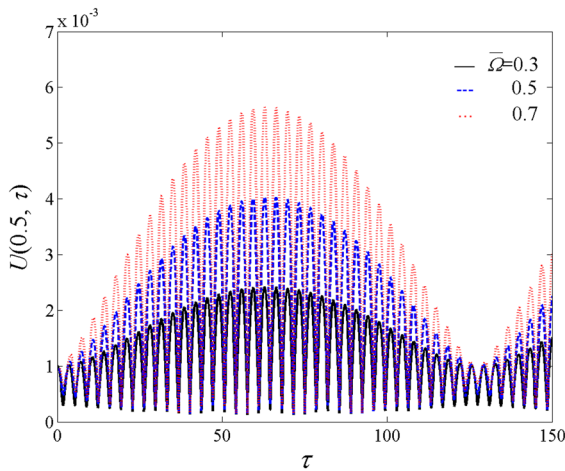


Fig. 7 Dynamic responses of transverse displacements under different speeds with $\theta/2\omega = 0.9$ $\alpha = 0.38$

determined by Floquet’s and Bolotin’s methods are also plotted. It is observed from Fig. 6a that parametric instability regions determined by DSC and Floquet’s methods are ‘V’ shapes, and do not vary obviously with spinning speed increasing, which means spinning speed has no significant influence on parametric instability regions of rotating shafts without damping. While seen from Fig. 6b, parametric instability regions determined by Bolotin’s method expand with spinning speed increasing [1–3, 6, 7], which contradict the present numerical results by DSC and those by Floquet’s method. From the above comparison and contrast, it may be considered that the present numerical results obtained by DSC support Floquet’s method, but disagree with Bolotin’s method. In the work of Pei [18], Bolotin’s method is considered to result in the enlargement of instability regions for rotating systems, and may be considered to be not adapted to parametric instability analysis of rotating systems. The present study further validates the viewpoint in the work of Pei by using a direct numerical simulation method, rather than a theoretical method. Especially, to the authors’ knowledge, there are no experimental reports on this problem. Therefore, this numerical study appears especially important to enhance understanding parametric instability of rotating systems.

Figure 7 shows dimensionless displacements of midpoint on the shaft under different spinning speeds with $\theta/2\omega = 0.9$ $\alpha = 0.38$. It is found that the amplitudes of displacements increase with spinning

speed increasing. Therefore, it may be considered that the increase of spinning speed does not affect the size of parametric instability regions of rotating shafts with no damping obviously, while results in the increase of the amplitude of displacement.

3.2 Parametric instability regions for shafts with damping

In this sub-section, effects of spinning speed on parametric instability regions of rotating shafts with external viscous damping and internal material damping are discussed. And influence of increase of damping on parametric instability regions is also analyzed.

Figure 8 shows dynamic responses of dimensionless displacements at midpoint for a rotating shaft with spinning speed $\bar{\Omega} = 0.3$ and external damping $\zeta_e = 0.05$. It is seen that the dynamic responses for $\theta/2\omega = 1.0$ $\alpha = 0.20$, and $\theta/2\omega = 0.9$ $\alpha = 0.42$ from Figs. 8b, d, are dynamically unstable; while the dynamic responses for $\theta/2\omega = 1.0$ $\alpha = 0.18$ and $\theta/2\omega = 0.9$ $\alpha = 0.40$ from Fig. 8a, c, reduce with time increasing, and are dynamically stable. The whole procedure above is repeated, then the parametric instability region with $\bar{\Omega} = 0.3$, $\zeta_e = 0.05$ shown as Fig. 9 is plotted. Similarly, the parametric instability regions with different spinning speeds $\bar{\Omega} = 0.5$ and 0.7 for rotating shafts with damping $\zeta_e = 0.05$ are presented in Figs. 10 and 11. In order to analyze damping effects, the instability regions for rotating shafts with no damping are also plotted in Figs. 9, 10 and 11.

In Figs. 9, 10 and 11, it is found that the parametric instability regions determined by DSC algorithm agree well with those determined by Floquet’s method, respectively, although there are some errors. It is also observed from Figs. 9, 10 and 11 that the boundaries of parametric instability regions for a rotating shaft with external damping intersect with those for a rotating shaft with no damping in certain cases, respectively. Furthermore, this phenomenon gets more obvious with spinning speed increasing, and is quite different from that for non-spinning beams. According to conclusions in the book of Bolotin [24], the boundaries of parametric instability regions for beams with external damping are included in those for beams with no damping, and these two kinds of

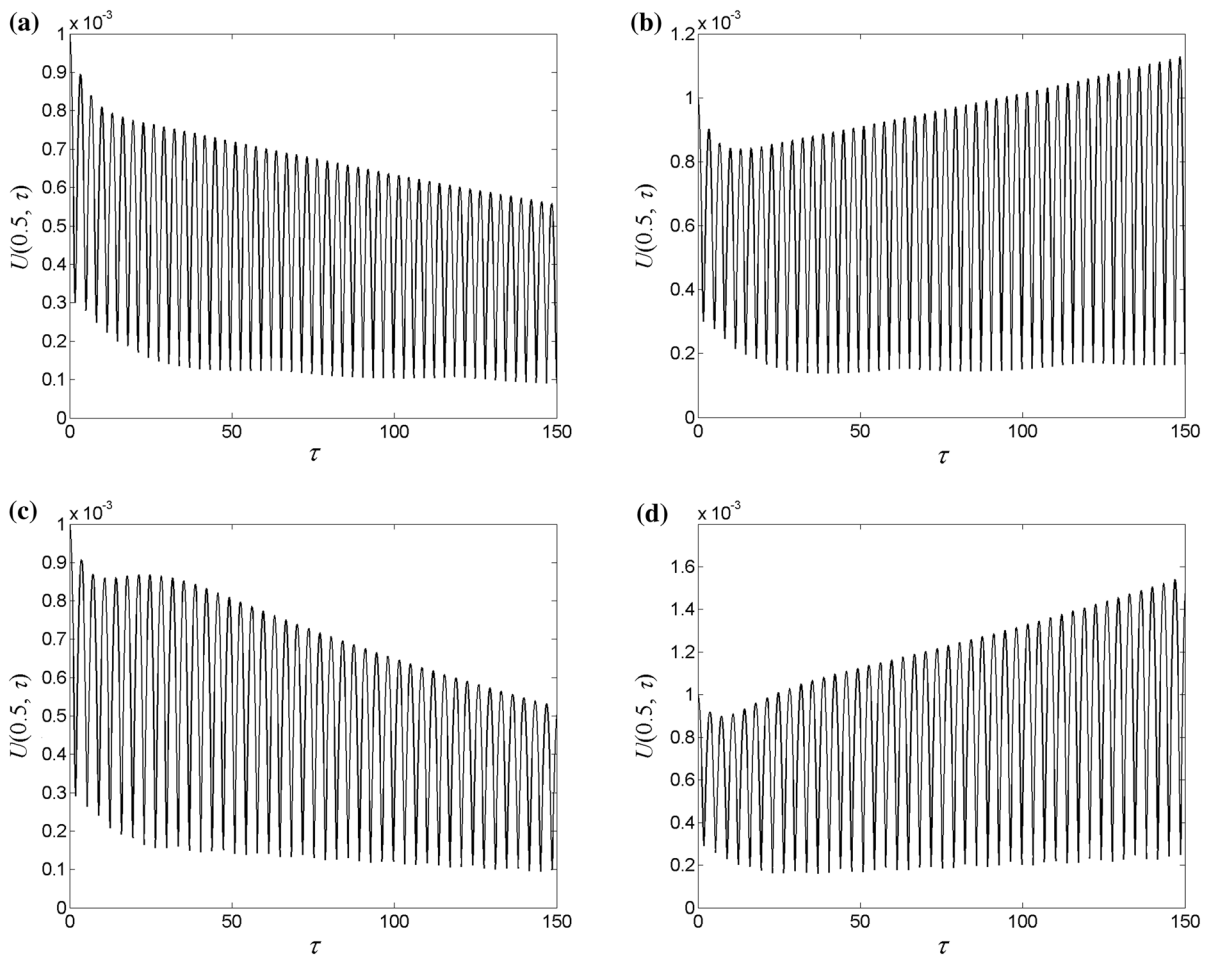


Fig. 8 Dynamic responses of transverse dimensionless displacements for a rotating shaft with external damping $\zeta_e = 0.05$ and spinning speed $\bar{\Omega} = 0.3$. **a** $\theta/2\omega = 1.0$ $\alpha = 0.18$, **b** $\theta/2\omega = 1.0$ $\alpha = 0.20$, **c** $\theta/2\omega = 0.9$ $\alpha = 0.40$, **d** $\theta/2\omega = 0.9$ $\alpha = 0.42$

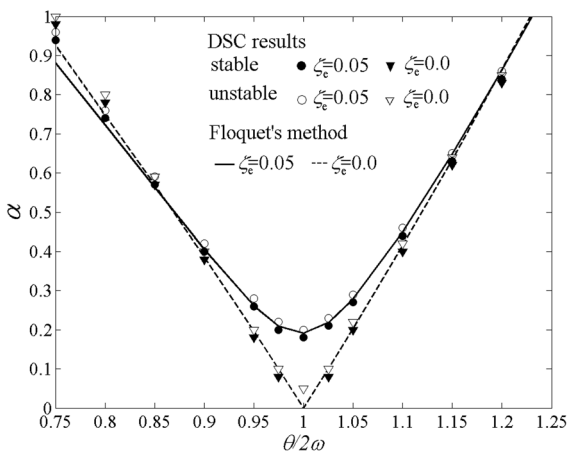


Fig. 9 Dynamic instability region of a rotating shaft with $\bar{\Omega} = 0.3$ $\zeta_e = 0.05$

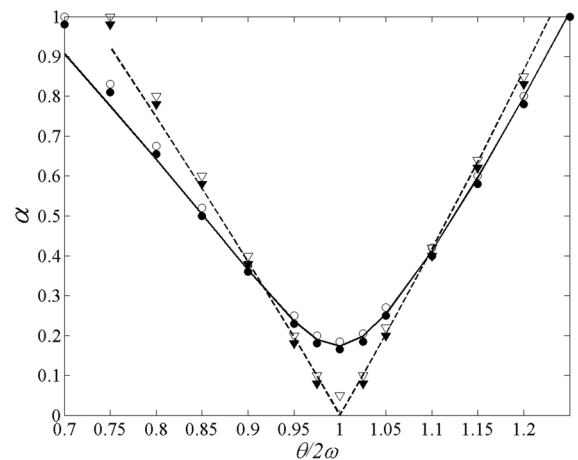


Fig. 10 As Fig. 9, but $\bar{\Omega} = 0.5$, Key as for Fig. 9

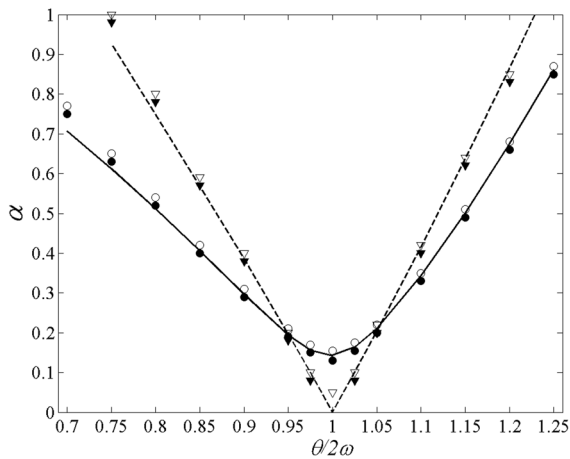


Fig. 11 As Fig. 9, but $\bar{\Omega} = 0.7$, Key as for Fig. 9

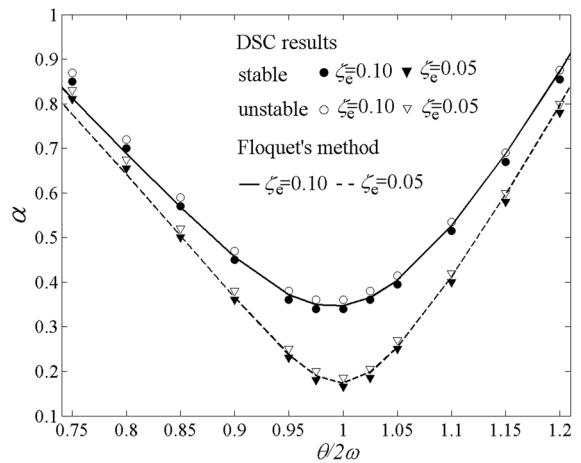


Fig. 13 Effects of the increase of damping on parametric instability regions with $\bar{\Omega} = 0.5$

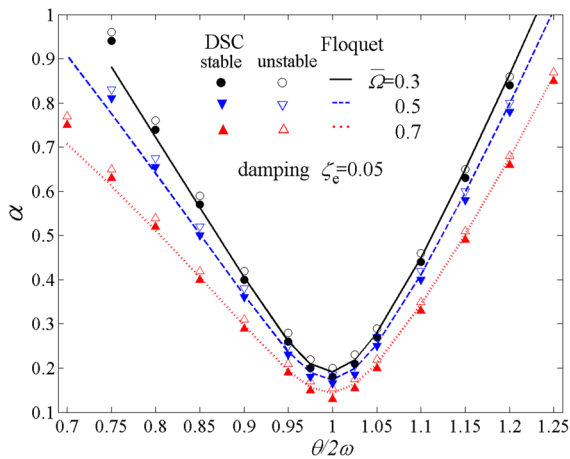


Fig. 12 Effects of spinning speed on parametric instability regions for a rotating shaft with external damping $\zeta_e = 0.05$

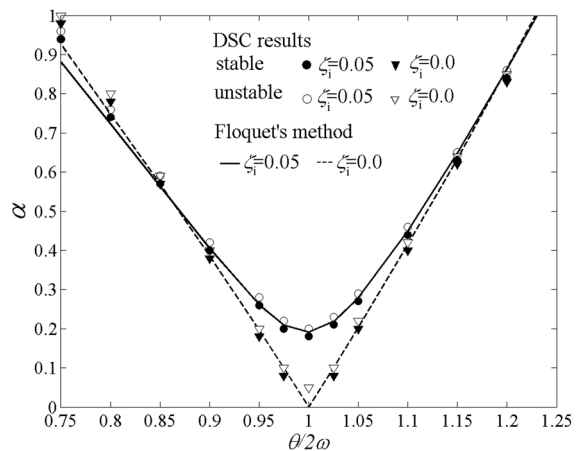


Fig. 14 Dynamic instability region of a rotating shaft with $\bar{\Omega} = 0.3$ $\zeta_i = 0.05$

boundaries cannot intersect each other. To the authors' knowledge, this phenomenon for rotating shafts has not been reported in the published works [1–3, 6, 7]. Therefore, this phenomenon is a new found, which can enhance more understanding to parametric instability of rotating systems. However, on the cause of this phenomenon, further investigation on this problem is needed.

A comparison of parametric instability regions with different spinning speeds for rotating shafts with external damping $\zeta_e = 0.05$ is shown in Fig. 12. It is found that the instability regions for rotating shafts with damping determined by DSC and Floquet's method are enlarged as spinning speed increases,

which means that the increase of spinning speed leads to enlargement of instability regions for rotating shafts with damping, but has little influence on instability regions for rotating shafts without damping seen from Fig. 6. Therefore, due to the existence of damping, spinning speed has a significant influence on parametric instability regions of rotating shafts. In addition, effect of the increase of damping on parametric instability regions is demonstrated in Fig. 13. It is seen that the increase of damping results in the reduction of parametric instability region, which improves dynamic stability of systems. And the effect is very obvious when the exciting frequency is near twice of the natural frequency.

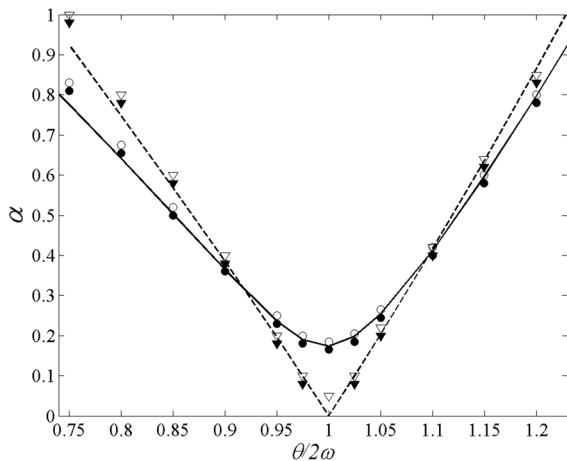


Fig. 15 As Fig. 14, but $\bar{\Omega} = 0.5$, Key as for Fig. 14

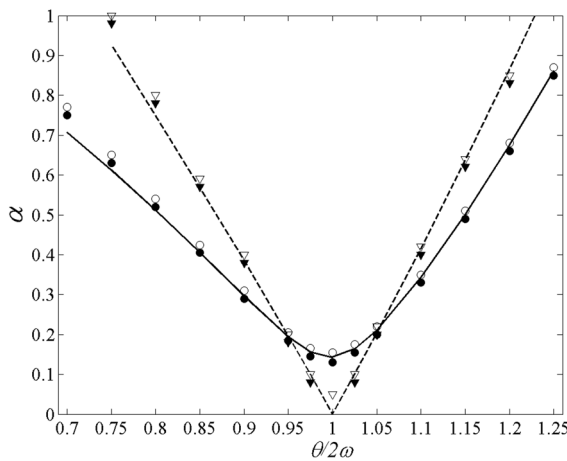


Fig. 16 As Fig. 14, but $\bar{\Omega} = 0.7$, Key as for Fig. 14

Parametric instability regions of rotating shafts with internal material damping under different spinning speeds are plotted in Figs. 14, 15 and 16. Similarly to Figs. 9, 10 and 11, it is observed from Figs. 14, 15 and 16 that the boundaries of parametric instability regions for rotating shafts with internal damping intersect with those for rotating shafts with no damping, respectively. Moreover, this phenomenon gets more obvious as spinning speed increases. Figure 17 shows the comparison of parametric instability regions with different spinning speeds for rotating shafts with internal damping $\zeta_i = 0.05$. It is found that the instability regions are enlarged as spinning speed increases, that is to say the

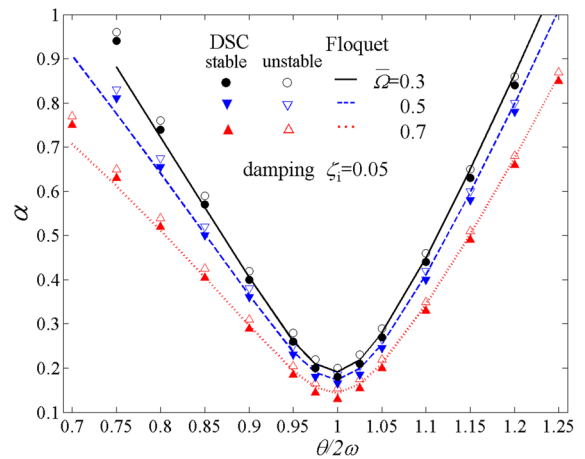


Fig. 17 Effects of spinning speed on parametric instability regions for a rotating shaft with internal damping $\zeta_i = 0.05$

increase of spinning speed leads to enlargement of instability regions for rotating shafts with internal material damping. These above conclusions are similar to those for rotating shafts with external damping, which means internal material damping has the same influence on parametric instability regions of rotating shafts as external viscous damping.

4 Conclusions

Parametric instability of a rotating shaft with different spinning speeds subjected to a periodic axial force has been studied by using DSC method. External viscous damping and internal material damping (Voigt–Kelvin model) are considered. Effects of spinning speed and damping on parametric instability regions for rotating shafts also have been investigated. The following conclusions may have been drawn.

1. For rotating shafts with no damping, parametric instability regions with different spinning speeds determined by DSC method are ‘V’ shapes, and do not vary obviously with spinning speed increasing, which agree well with those determined by Floquet’s method, but are quite different from those determined by Bolotin’s method. It may be considered that the numerical results obtained by DSC method support Floquet’s method, disagree with Bolotin’s method, and further validate the viewpoint in the work of Pei

[18]. Therefore, it is strongly recommended that Bolotin's method should not be applied to parametric instability analysis for rotating systems. Moreover, considering that experimental reports on this problem have not been published, this present numerical study appears especially important to help us to better understand parametric instability of rotating systems.

2. For rotating shafts with damping, the effects of external viscous damping and internal material damping on parametric instability regions are similar. Parametric instability regions under different spinning speeds determined by DSC method are enlarged significantly as spinning speed increases, that is to say the increase of spinning speed results in the enlargement of instability region, which are in good agreement with those obtained by Floquet's method. The present results further support Floquet's method. In addition, the increase of damping results in reduction of parametric instability region, which is helpful to improve dynamic stability of rotating systems, especially when the exciting frequency is near twice of the natural frequency.
3. The boundaries of parametric instability regions for a rotating shaft with damping (external and internal damping) intersect with those for a rotating shaft with no damping in certain cases, respectively. Moreover, this phenomenon gets more obvious with spinning speed increasing, which is quite different from that for non-spinning beams. This phenomenon has not been studied in the published works, which can enhance more understanding to parametric instability of rotating systems.
4. The effects of spinning speed on parametric instability regions are different from those in some published works. It may be considered that spinning speed has no significant influence on parametric instability regions for rotating shafts with no damping, while has a great effect on parametric instability regions for rotating shafts with damping including external and internal damping. The parametric instability regions for rotating shafts with damping are enlarged significantly as spinning speed increases. Of course, the spinning speed considered here is lower to the critical spinning speed.
5. Parametric instability regions are determined by judging stability of displacement responses

obtained by using DSC procedure to directly solve governing differential equations of rotating shafts, which is quite different from the way by using theoretical methods. The present study further validates the viewpoint in the work of Pei by using a direct simulation method–DSC, rather than a theoretical method.

6. This study extends the application field of DSC method from vibration and buckling analysis of beams (boundary-value problem) to dynamic response solution and parametric instability analysis of rotating shafts (initial-value problem). The calculation procedure for solving governing differential equations of rotating shafts can also be used to solve other problems.

References

1. Chen LW, Ku DM (1990) Dynamic stability analysis of a rotating shaft by the finite element method. *J Sound Vib* 143(1):143–151
2. Chen LW, Ku DM (1991) Dynamic stability of a rotating shaft embedded in an isotropic Winkler-type foundation. *Mech Mach Theory* 26(7):687–696
3. Chen LW, Ku DM (1992) Dynamic stability of a cantilever shaft–disk system. *J Vib Acoust Trans ASME* 114(3):326–329
4. Lee HP (1995) Dynamic stability of spinning pre-twisted beams subject to axial pulsating loads. *Comput Methods Appl Mech Eng* 127(1–4):115–126
5. Lee HP (1995) Effects of axial base excitations on the dynamic stability of spinning pre-twisted cantilever beams. *J Sound Vib* 185(2):265–278
6. Chen LW, Peng WK (1998) Dynamic stability of rotating composite shafts under periodic axial compressive loads. *J Sound Vib* 212(2):215–230
7. Sheu HC, Chen LW (2000) A lumped mass model for parametric instability analysis of cantilever shaft–disk systems. *J Sound Vib* 234(2):331–348
8. Lin CY, Chen LW (2005) Dynamic stability of spinning pre-twisted sandwich beams with a constrained damping layer subjected to periodic axial loads. *Compos Struct* 70(3):275–286
9. Liao CL, Huang BW (1995) Parametric instability of a spinning pretwisted beam under periodic axial force. *Int J Mech Sci* 37(4):423–439
10. Liao CL, Huang BW (1995) Parametric resonance of a spinning pretwisted beam with time-dependent spinning rate. *J Sound Vib* 180(1):47–65
11. Tan TH, Lee HP, Leng GSB (1997) Parametric instability of spinning pretwisted beams subjected to spin speed perturbation. *Comput Methods Appl Mech Eng* 148(1–2):139–163
12. Tan TH, Lee HP, Leng GSB (1998) Parametric instability of spinning pretwisted beams subjected to sinusoidal compressive axial loads. *Comput Struct* 66(6):745–764

13. Yoon SJ, Kim JH (2002) A concentrated mass on the spinning unconstrained beam subjected to a thrust. *J Sound Vib* 254(4):621–634
14. Young TH, Gau CY (2003) Dynamic stability of spinning pretwisted beams subjected to axial random forces. *J Sound Vib* 268(1):149–165
15. Young TH, Gau CY (2003) Dynamic stability of pre-twisted beams with non-constant spin rates under axial random forces. *Int J Solids Struct* 40(18):4675–4698
16. Pavlović R, Rajković P, Pavlović I (2008) Dynamic stability of the viscoelastic rotating shaft subjected to random excitation. *Int J Mech Sci* 50(2):359–364
17. Pavlović R, Rajković P, Mitić S, Pavlović I (2009) Stochastic stability of a rotating shaft. *Arch Appl Mech* 79(12):1163–1171
18. Pei YC (2009) Stability boundaries of a spinning rotor with parametrically excited gyroscopic system. *Eur J Mech A Solids* 28(4):891–896
19. Chen WR (2010) Parametric instability of spinning twisted Timoshenko beams under compressive axial pulsating loads. *Int J Mech Sci* 52(9):1167–1175
20. Younesian D, Esmailzadeh E (2010) Nonlinear vibration of variable speed rotating viscoelastic beams. *Nonlinear Dyn* 60(1–2):193–205
21. Shahgholi M, Khadem SE (2012) Stability analysis of a nonlinear rotating asymmetrical shaft near the resonances. *Nonlinear Dyn* 70(2):1311–1325
22. Shahgholi M, Khadem SE, Bab S (2015) Nonlinear vibration analysis of a spinning shaft with multi-disks. *Meccanica* 50:2293–2307. doi:[10.1007/s11012-015-0154-8](https://doi.org/10.1007/s11012-015-0154-8)
23. Li W, Song ZW, Gao XX, Chen ZG (2015) Dynamic instability analysis of a rotating ship shaft under a periodic axial force by discrete singular convolution. *Shock Vib*. doi:[10.1155/2015/482607](https://doi.org/10.1155/2015/482607)
24. Bolotin VV (1965) *The dynamic stability of elastic systems*. Holden-Day Inc, New York
25. Nayfeh AH, Mook DT (1995) *Nonlinear oscillation*. Wiley, New York
26. Iwatsubo T, Sugiyama Y, Ishihara K (1972) Stability and non-stationary vibration of columns under periodic loads. *J Sound Vib* 23(2):245–257
27. Song ZW, Li W, Liu GR (2012) Stability and non-stationary vibration analysis of beams subjected to periodic axial forces using discrete singular convolution. *Struct Eng Mech* 44(4):487–499
28. Li W, Song ZW, Chai YB (2015) Discrete singular convolution method for dynamic stability analysis of beams under periodic axial forces. *J Eng Mech*. doi:[10.1061/\(ASCE\)EM.1943-7889.0000931](https://doi.org/10.1061/(ASCE)EM.1943-7889.0000931)
29. Song ZW, Chen ZG, Li W, Chai YB (2015) Dynamic stability analysis of beams with shear deformation and rotary inertia subjected to periodic axial forces by using discrete singular convolution method. *J Eng Mech*. doi:[10.1061/\(ASCE\)EM.1943-7889.0001023](https://doi.org/10.1061/(ASCE)EM.1943-7889.0001023)
30. Wei GW (1999) Discrete singular convolution for the solution of the Fokker–Planck equations. *J Chem Phys* 110(18):8930–8942
31. Wei GW (2000) Discrete singular convolution for the sine-Gordon equation. *Phys D* 137(3–4):247–259
32. Feng BF, Wei GW (2002) A comparison of the spectral and the discrete singular convolution schemes for the KdV-type equations. *J Comput Appl Math* 145(1):183–188
33. Yang SY, Zhou YC, Wei GW (2002) Comparison of the discrete singular convolution algorithm and the Fourier pseudospectral method for solving partial differential equations. *Comput Phys Commun* 143(2):113–135
34. Ng CHW, Zhao YB, Wei GW (2004) Comparison of discrete singular convolution and generalized differential quadrature for the vibration analysis of rectangular plates. *Comput Methods Appl Mech Eng* 193(23–26):2483–2506
35. Du H, Lim MK, Lin RM (1994) Application of generalized differential quadrature method to structure problems. *Int J Numer Methods Eng* 37(11):1881–1896
36. Zienkiewicz OC, Taylor RL (1989) *The finite element method*, vol 1. McGraw-Hill, New York
37. Wei GW, Zhao YB, Xiang Y (2002) A novel approach for the analysis of high-frequency vibrations. *J Sound Vib* 257(2):207–246
38. Zhao YB, Wei GW, Xiang Y (2002) Discrete singular convolution for the prediction of high frequency vibration of plates. *Int J Solids Struct* 39(1):65–88
39. Wei GW (2001) Vibration analysis by discrete singular convolution. *J Sound Vib* 244(3):535–553
40. Wei GW (2001) Discrete singular convolution for beam analysis. *Eng Struct* 23(9):1045–1053
41. Zhao S, Wei GW, Xiang Y (2005) DSC analysis of free-edged beams by an iteratively matched boundary method. *J Sound Vib* 284(1–2):487–493
42. Wei GW (2001) A new algorithm for solving some mechanical problems. *Comput Methods Appl Mech Eng* 190(15–17):2017–2030
43. Wei GW, Zhao YB, Xiang Y (2001) The determination of natural frequencies of rectangular plates with mixed boundary conditions by discrete singular convolution. *Int J Mech Sci* 43(8):1731–1746
44. Zhao YB, Wei GW (2002) DSC analysis of rectangular plates with non-uniform boundary conditions. *J Sound Vib* 255(2):203–228
45. Wei GW, Zhao YB, Xiang Y (2002) Discrete singular convolution and its application to the analysis of plates with internal supports. Part 1: theory and algorithm. *Int J Numer Methods Eng* 55(8):913–946
46. Xiang Y, Zhao YB, Wei GW (2002) Discrete singular convolution and its application to the analysis of plates with internal supports. Part 2: applications. *Int J Numer Methods Eng* 55(8):947–971
47. Zhao YB, Wei GW, Xiang Y (2002) Plate vibration under irregular internal supports. *Int J Solids Struct* 39(5):1361–1383
48. Yu SN, Xiang Y, Wei GW (2009) Matched interface and boundary (MIB) method for the vibration analysis of plates. *Commun Numer Methods Eng* 25(9):923–950
49. Civalek Ö (2007) Three-dimensional vibration, buckling and bending analyses of thick rectangular plates based on discrete singular convolution method. *Int J Mech Sci* 49(6):752–765
50. Civalek Ö (2009) Fundamental frequency of isotropic and orthotropic rectangular plates with linearly varying

- thickness by discrete singular convolution method. *Appl Math Model* 33(10):3825–3835
51. Civalek Ö (2008) Free vibration analysis of symmetrically laminated composite plates with first-order shear deformation theory (FSDT) by discrete singular convolution method. *Finite Elem Anal Des* 44:725–731
 52. Civalek Ö (2006) An efficient method for free vibration analysis of rotating truncated conical shells. *Int J Press Vessels Pip* 83(1):1–12
 53. Civalek Ö (2007) A parametric study of the free vibration analysis of rotating laminated cylindrical shells using the method of discrete singular convolution. *Thin Walled Struct* 45(7–8):692–698
 54. Civalek Ö (2007) Numerical analysis of free vibrations of laminated composite conical and cylindrical shells: discrete singular convolution (DSC) approach. *J Comput Appl Math* 205(1):251–271
 55. Civalek Ö (2013) Vibration analysis of laminated composite conical shells by the method of discrete singular convolution based on the shear deformation theory. *Compos B Eng* 45:1001–1009
 56. Wang XW, Xu SM (2010) Free vibration analysis of beams and rectangular plates with free edges by the discrete singular convolution. *J Sound Vib* 329(10):1780–1792
 57. Xu SM, Wang XW (2011) Free vibration analyses of Timoshenko beams with free edges by using the discrete singular convolution. *Adv Eng Softw* 42(10):797–806
 58. Zhu Q, Wang XW (2011) Free vibration analysis of thin isotropic and anisotropic rectangular plates by the discrete singular convolution algorithm. *Int J Numer Methods Eng* 86(6):782–800
 59. Duan GH, Wang XW (2013) Free vibration analysis of multiple-stepped beams by the discrete singular convolution. *Appl Math Comput* 219(24):11096–11109
 60. Duan GH, Wang XW (2014) Vibration analysis of stepped rectangular plates by the discrete singular convolution algorithm. *Int J Mech Sci* 82:100–109
 61. Lim CW, Li ZR, Wei GW (2005) DSC-Ritz method for high-mode frequency analysis of thick shallow shells. *Int J Numer Methods Eng* 62(2):205–232
 62. Hou Y, Wei GW, Xiang Y (2005) DSC-Ritz method for the free vibration analysis of Mindlin plates. *Int J Numer Methods Eng* 62(2):262–288
 63. Xiang Y, Lai SK, Zhou L (2010) DSC-element method for free vibration analysis of rectangular Mindlin plates. *Int J Mech Sci* 52(4):548–560
 64. Wan DC, Wei GW (2000) The Study of quasi-wavelets based numerical method applied to Burgers' equations. *Appl Math Mech Engl Ed* 21(10):1099–1110
 65. Xiong W, Zhao YB, Gu Y (2003) Parameter optimization in the regularized Shannon's kernels of higher-order discrete singular convolutions. *Commun Numer Methods Eng* 19(5):377–386